

# Process and Microstructure in Materials-Affected Manufacturing

Steven Y. Liang and Zhipeng Pan

**Abstract** The fundamental understanding of manufacturing processes has been long focused on the geometric, mechanic, and thermal aspects leading to the product shape and finish. However, the effects of process mechanics attributing to material microstructural properties and constitutive characteristics are essential but not yet well understood due to the intricacy of multiple scale process-materials interaction physics. Further, the effects of materials mechanics on the process behaviors, in the context of stress and heat generations, carries significant practical relevance but has not been fully addressed in science. This is to state that manufacturing processes, such as metal forging, polymer compression modeling, 3-D printing, et al., commonly involve a significant amount of mechanical, thermal, and even chemical loadings that interact strongly with part material microstructural evolutions, which in turn determine the performance and functionality beyond just the shape and finish of the end products. On the other hand, the materials microstructure in terms of grain size, texture, phase field, etc. can also change the stress and heat generation mechanics of the manufacturing process. The scope of this paper is to present the “materials-affected manufacturing” connotation in exploring how process mechanics and materials mechanics interact retroactively with each other, and based upon this connotation better predictions of force, temperature, residual stress, and final part properties and functionalities can be possible. The materials-affected manufacturing analysis methodology involves an iterative blending scheme in combining microstructural synthesis and material homogenization analysis to allow for the interactive effects of materials dynamics and processing mechanics to be considered simultaneously. This paper discusses the basic formulation, computational configuration, and experimental validation in the example cases of machining operations with material recrystallization, grain size variation, recrystallization, texture, and phase field in consideration. Explicit calculation of material microstructure evolution path is provided as functions of process parameters and materials attributes. To factor the material microstructure

---

S.Y. Liang (✉) · Z. Pan

Woodruff School of Mechanical Engineering, Georgia Institute  
of Technology, Atlanta, GA 30332, USA  
e-mail: steven.liang@me.gatech.edu

© Springer International Publishing AG 2017

V. Majstorovic and Z. Jakovljevic (eds.), *Proceedings of 5th International  
Conference on Advanced Manufacturing Engineering and Technologies*,  
Lecture Notes in Mechanical Engineering, DOI 10.1007/978-3-319-56430-2\_23

309

states into the thermo-mechanical coupling process, the material microstructure terms are introduced into the traditional material constitutive model with hardened steels and titanium alloys as examples. Results show that residual stresses and machining forces can be better modeled and predicted in the materials-affected manufacturing analysis platform.

**Keywords** Machining · Microstructure · Flow stress · Force · Residual stress

## 1 Introduction

The development of high precision machining technology enables the complicated shape control, high geometrical accuracy and good surface integrity of the end product [1–3]. The geometrical shape control is achieved by the precise machine tool path planning and error compensation. Appropriate design of the final workpiece material mechanical and microstructural property is required for good surface integrity. The machining process conditions could significantly influence the resultant surface integrity of the final workpiece material. The service functionality of the precision machining end product strongly depends on workpiece material properties. The main consideration in terms of the final workpiece properties includes mechanical attributes (residual stress profile, yield stress, surface hardness), microstructure states (grain structure and orientation, phase composition). The workpiece material properties in the machining process are directly influenced by the process conditions.

Appropriate selection of the machining parameters could help to improve the functionality performance of the end product [4]. For the hard to machine material, such as titanium, nickel based alloys and hardened steels, the high precision machining still faces considerable challenges [5–7]. Significant microstructural evolution has been observed in the machining process [8–10]. The material mechanical properties are strongly dependent on the microstructural states. Also workpiece surface corrosion resistance, microhardness are also influenced by the microstructural attributes. The machining induced residual stress profile is a critical factor for the workpiece corrosion resistance. For biomedical or aerospace industry, the grain refinement would be desirable for the strengthening.

The thermo-mechanical loading introduced from high speed machining will unfavorably affect the workpiece material properties, such as augmented grain size, reduced surface hardness, and tensile residual stress profile [11, 12]. Most of the current research work only focuses on the thermo-mechanical coupling process, where the microstructural evolution effect is largely ignored. However, obvious microstructural change has been observed in the machining process, especially for multiphase material, such as titanium alloys and nickel based alloys. Therefore, it is important to understand the thermo-mechanical-microstructural coupling effects.

The combined effect of severe plastic deformation, large strain, high strain rate and high temperature in the primary shear zone and workpiece/tool interface would promote the microstructure evolution such as dislocation density change, grain size

evolution and multiphase material phase transformation. The early work on the microstructure change in the machining process is reported by Xu et al. [13] in the grinding of ceramics. The different material microstructure effect on the material removal mechanism is investigated. The white layer is observed in the hard turning of hardened steel by Chou et al. [14], which results from workpiece material phase transformation effect. Similarly, the extensive grain refinement and strain induced martensite phase transformation is observed by Ghosh et al. [9] in surfaced turning of 304L stainless steel. The grain refinement and uniform nanocrystalline structure also is found in the chip in turning of copper by Swaminathan et al. [15].

The investigation of machining induced microstructure change would not only benefit the machining process optimization to achieve machining end product with good service functionality, the machining tool selection and improvement could also be obtained. However, the microstructural level investigation of machining is still at its debut stage, where most of the research focuses on the experimental investigation. The aim of the current paper is to summarize the current existing research work on the machining induced microstructure change and discuss a computational frame work for the machining induced microstructure evolution investigation. The case studies are proposed in hardened steels and titanium alloys.

## 2 Microstructure Evolution Modeling

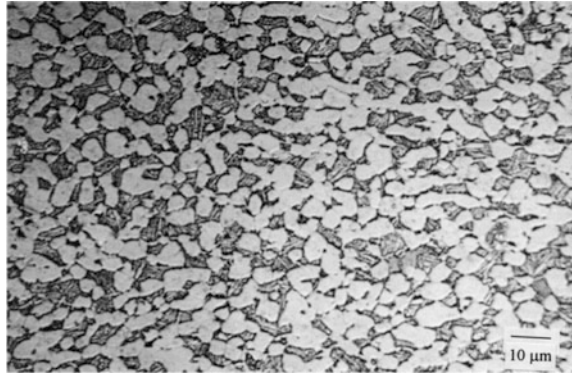
### 2.1 Phase Transformation and Dynamic Recrystallization of *Ti-6Al-4V*

Titanium alloys could be divided into three types based on the crystal structure,  $\alpha$  alloys,  $\beta$  alloys and  $\alpha + \beta$  alloys [16]. The  $\alpha$  alloys have  $\alpha$  stabilizer such as aluminum and tin with a *hcp* structure at the room temperature. High strength, toughness are the main characters of  $\alpha$  alloys. The  $\beta$  alloys are in the state of *bcc* phase which contains large amount of  $\beta$  isomorphous additions, such as vanadium, niobium and tantalum. The low strength characterizes the basic mechanical property of the  $\beta$  alloys. For the  $\alpha + \beta$  alloys, more than one  $\alpha$  stabilizers together with  $\beta$  stabilizers exist. The adjustment of the microstructural states could control the mechanical properties of  $\alpha + \beta$  alloys. So various heat treatment method could control the strength and fracture toughness of the material in a wide range.

*Ti-6Al-4V* is a typical  $\alpha + \beta$  alloy, which contains 6 wt%  $\alpha$  phase stabilizing aluminum and 4 wt%  $\beta$  phase stabilizing vanadium. The equilibrium state microstructure contains the *hcp* structured  $\alpha$  phase with scattered distribution of  $\beta$  phase at the room temperature, as shown in Fig. 1 [17]. The microstructure property may vary depending on the prior heat treatment. Basic microstructural types in *Ti-6Al-4V* includes grain boundary allotriomorph, primary  $\alpha$ , Widmanstätten and martensitic. The cooling rate could greatly influence  $\beta$  precipitates distribution and morphology.

The mechanical properties of the *Ti-6Al-4V* material are dependent on the microstructural states. The dominating factor that influences the mechanical

**Fig. 1** Typical microstructure of *Ti-6Al-4V* alloy [17]



properties is the  $\alpha$  phase colony size. The yield strength, fracture toughness and ductility could be greatly improved by reducing the colony size of  $\alpha$  phase.

The JMAK model has been widely used to describe the dynamic recrystallization process of crystalline material by considering the strain, strain rate and temperature [18]. The basics of *JMAK* model is the calculation of the recrystallized volume fraction of the material as a function of time. The grain size is obtained from the grain growth rate and nucleation. The dynamic recrystallization is defined with the Avrami equation as

$$X_{drex} = 1 - \exp \left[ -\beta_d \left( \frac{\varepsilon - a_{10}\varepsilon_p}{\varepsilon_{0.5}} \right)^{k_d} \right] \quad (1)$$

where  $\varepsilon$  is the strain,  $\varepsilon_p$  is the peak strain,  $X_{drex}$  is the volume fraction of dynamically recrystallized material.  $\varepsilon_{0.5}$  is the strain for  $X_{drex} = 0.5$  and it is given by

$$\varepsilon_{0.5} = a_5 d_0^{h_5} \dot{\varepsilon}^{n_5} \dot{\varepsilon}^{m_5} \exp(Q_{act} m_5 / RT) + c_5 \quad (2)$$

where  $R$  is the gas constant,  $d_0$  is the initial diameter of the grain,  $a_5$ ,  $h_5$ ,  $n_5$ ,  $m_5$ ,  $c_5$  are material constants which could be determined by experiments and regression analysis,  $Q_{act}$  is the activation energy. A critical strain at which the dynamic recrystallization would occur is defined as  $\varepsilon_p = 0.8 \varepsilon_p$ . The peak strain  $\varepsilon_p$  is denoted as

$$\varepsilon_p = a_1 d_0^{h_1} \dot{\varepsilon}^{m_1} \exp(Q_{act} m_1 / RT) + c_1 \quad (3)$$

where  $a_1$ ,  $h_1$ ,  $m_1$ ,  $c_1$  are material constants. The grain size after recrystallization is given by

$$d_{drex} = a_8 d_0^{h_8} \dot{\varepsilon}^{n_8} \dot{\varepsilon}^{m_8} \exp(Q_{act} m_8 / RT) + c_8 \quad (4)$$

where  $a_8$ ,  $h_8$ ,  $n_8$ ,  $m_8$ ,  $c_8$  are the material constants. The average grain size is calculated with a mixture rule as

**Table 1** JMAK parameters of *Ti-6Al-4V* material

Peak strain	$a_1$	$h_1$	$m_1$	$Q_{act}m_1$	$c_1$		$a_2$		
	0.0064	0	0.0801	30,579 J/mol	0		0.8		
DRx kinematics	$a_5$	$h_5$	$n_5$	$m_5$	$Q_{act}m_5$	$c_5$	$\beta_d$	$k_d$	$a_{10}$
	0.022	0	0	0.11146	26,430 J/mol	0	0.9339	0.5994	0.0311
DRx grain size	$a_8$	$h_8$	$n_8$	$m_8$	$Q_{act}m_8$	$c_8$			
	150	0	0	-0.03	-6540	0			

$$d = d_0(1 - X_{drex}) + d_{drex}X_{drex} \tag{5}$$

The initial average grain size is characterized as  $d_0 = 15 \mu\text{m}$ . The *JMAK* parameters of *Ti-6Al-4V* are listed in Table 1.

The microstructure modelling of *Ti-6Al-4V* consists of two phases,  $\alpha$  phase and  $\beta$  phase. The initial microstructure of *Ti-6Al-4V* is bimodal, mainly composed  $\alpha$  grains with low concentration of  $\beta$ . In the thermal heating process,  $\alpha$  destabilizes and the transformation from  $\alpha$  to  $\beta$  starts above the  $\beta$  transformation temperature according to the phase transformation curves. Also, in the cooling down process, the  $\beta$  phase starts to slowly decompose into  $\alpha$  phase. Therefore, two different  $\alpha$  phase need to be distinguished, Widmanstätten and grain boundary [19]. In the current study, to simplify the model, it is assumed that the material only consists of primary  $\alpha$  and  $\beta$  phase.

For the heating process where the phase transformation from  $\alpha$  to  $\beta$  takes place, a simplified Avrami model [20] is used as,

$$\vartheta_v = 1 - e^{\left\{A\left(\frac{T-T_s}{T_e-T_s}\right)^D\right\}} \tag{6}$$

where  $T$  is the temperature,  $T_s = 600 \text{ }^\circ\text{C}$  is the phase transformation starting temperature,  $T_e = 980 \text{ }^\circ\text{C}$  is the temperature when the process ends,  $A_s$  and  $D_s$  are material constants to be determined. The calculation of  $A_s$  and  $D_s$  could be conducted through an experimental curves of the phase transformation. In the current work,  $A_s$  and  $D_s$  are selected as  $-1.86$  and  $4.35$  from a previous study [21].

In the cooling down process, the  $\beta$  to  $\alpha + \beta$  transformation is characterized by the *TTT* curve, as shown in Fig. 2. As for the  $\alpha$  to  $\beta$  transformation in cooling, the coefficient is used as a mean value of a set of data from literature, which could be described by the function of time as

$$\xi = 1 - e^{-bT^n} \tag{7}$$

where  $b$  is the material constant and  $n = 1.32$  is the Avrami number. The dynamic recrystallization of the grain growth and phase transformation model are implemented in the finite element code for microstructural evolution simulation.

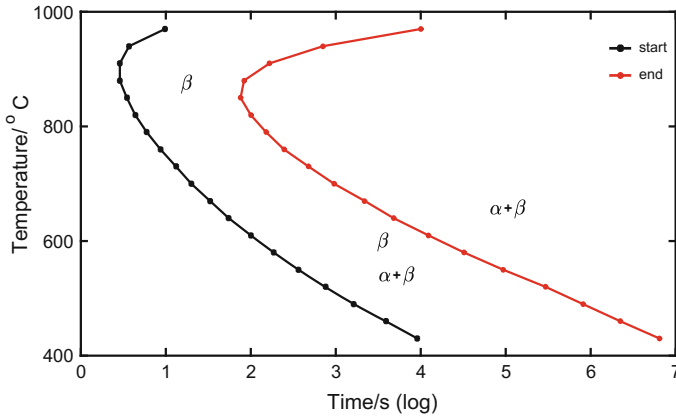
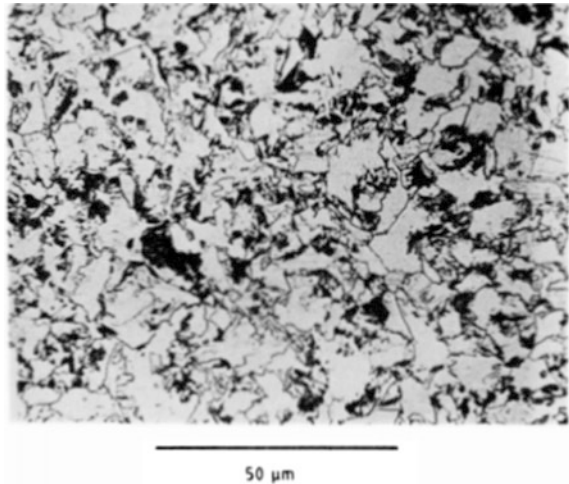


Fig. 2 The TTT curve of *Ti-6Al-4V*

## 2.2 Dynamic Recrystallization of 4130 Steel

AISI 4130 steel is a widely used hardened steel alloys because of its strong hardness and large yield strength. The grain structure of AISI 4130 steel is shown in Fig. 3[22]. The application of AISI 4130 steel includes bearing rings, transmission gears and crankshaft. However, those superior properties of AISI 4130 makes it hard to machining, which imposes great limitation on the material removal rate. The challenges in the machining of AISI 4130 steels comes from the large machining forces, bad surface quality, server tool wear and large dimensional distortion. A predictive force model scheme is proposed by Ji et al. [23] for the machining force optimization for orthogonal turning of AISI 4130. The effect of microstructure

Fig. 3 Typical microstructure of AISI 4130 steel alloys [22]



on machining force in turning of Al–Si alloys is investigated by Grum et al. [24]. Hodgson et al. [25] provides the models to predict  $X_{drex}$ , the recrystallized volume fraction, under static, dynamic and post dynamic recrystallization.  $X_{drex}$  is basically an exponential function of  $t/t_{0.5}$ .  $t$  is the time and  $t_{0.5}$  is the time of 50% softening for all steels.  $t_{0.5}$  is a function of inverse temperature. So based on the time and temperature during turning, the grain size drop could be calculated. Sun et al. [26] adopted empirical relationship to create a theoretical model to describe recrystallization kinetics. Later, Sajadi et al. [27] built the relationship between peak stress, temperature and strain rate. And the mean hot deformation activation energy  $Q_{act}$  of AISI 4130 was determined to calculate Zener-Hollomon parameter. The theory from these work is able to predict mechanical and thermal parameters but is not combined with classic machining theory. Current models [28–30] are able to predict forces in different materials including AISI 4130 but none of them take grain size change into consideration. With the similar approach for the *Ti–6Al–4V*, the average grain size could also be calculated in the machining process.

For the AISI 4130 steel, which is a C–Mn steel, the Sellar’s model [31] could be used in the form of,

$$d_{drex} = \varepsilon^{-0.5} d_0^{0.4} \exp\left(\frac{45,000}{RT}\right) \quad (8)$$

where  $\varepsilon$  is the plastic strain,  $d_0$  is the initial average grain size. The recrystallized volume fraction  $X_{drex}$  could be calculated as,

$$X_{drex} = 1 - \exp\left[-0.693\left(\frac{t}{t_{0.5}}\right)^{1.5}\right] \quad (9)$$

where  $t_{0.5}$  is the time when half of the material recrystallizes, defined as,

$$t_{0.5} = k_{md} Z^{n_{md}} \exp\left(\frac{Q_{md}}{RT}\right) \quad (10)$$

where  $k_{md}$ ,  $n_{md}$  and  $Q_{md}$  are material constants, selected as  $2.5 \times 10^{-6}$ ,  $-0.8$ , and  $230$  kJ/mol respectively;  $R$  is the universal gas constant,  $T$  is the temperature,  $Z$  is the Zener-Hollomon parameter defined as,

$$Z = \dot{\varepsilon} \exp\left(\frac{Q_{def}}{RT}\right) \quad (11)$$

where  $\dot{\varepsilon}$  is the plastic strain rate,  $Q_{def}$  is the material constant, selected to be  $300$  kJ/mol for all C–Mn alloy steels [31]. The *JMAK* parameters are taken from Hodgson’s [25] experimental measurement, which are listed in Table 2.

**Table 2** The JMAK parameters for AISI 4130 steel

$k_{md}$	$n_{md}$	$Q_{md}$	$Q_{def}$
$2.5 \times 10^{-6}$	-0.8	230 kJ/mol	300 kJ/mol

### 3 Microstructure Sensitive Flow Stress Model

The  $JC$  constitutive material flow stress model has been widely used in the machining process [32], which could be denoted as

$$\sigma = (A + B\varepsilon^n) \left[ 1 + C \ln \left( \frac{\dot{\varepsilon}}{\dot{\varepsilon}_0} \right) \right] \left\{ 1 - \left[ \frac{T - T_0}{T_m - T_0} \right]^m \right\} \quad (12)$$

where  $A$ ,  $B$ ,  $C$ ,  $m$ ,  $n$  are materials constants,  $\varepsilon$  is the equivalent plastic strain,  $\dot{\varepsilon}$  is equivalent strain rate,  $\dot{\varepsilon}_0$  is the reference strain rate, typically taken as  $1 \text{ s}^{-1}$ ,  $T$  is the material temperature,  $T_m$  is the material melting temperature and  $T_r$  is the room temperature. Since the  $JC$  model is purely based on experiment and data fitting, a lot of modified  $JC$  models have been developed to more accurately capture the material flow stress from the physical side of material deformation process. To account for the temperature dependent flow softening at high temperature, Calamaz et al. [33] suggested a strain and temperature tangent term. A later self-consistent model (SCM) is proposed by Zhang et al. [34] to account for the phase transformation in the dual phase  $Ti-6Al-4V$ . However, the SCM does not explicitly calculate the phase transformation and is only based on an iterative fitting method.

The flow stress of the dual-phase  $Ti-6Al-4V$  depends strongly on its microstructure. Due to increased temperature in the machining process, significant microstructure evolution could occur [35]. The grain morphology and volume fraction of different phase can vary significantly depending on the machining condition. The hexagonal  $\alpha$  phase has much stronger yield stress than the BCC  $\beta$  phase. The room temperature yield stress of  $Ti-6Al-4V$  can vary from 850 MPa to 1100 MPa in different heat treatment conditions. So, a reasonable flow stress model for  $Ti-6Al-4V$  should include the initial volume fraction of the two phases and the phase transformation in the machining process.

In the current study, since the volume fraction of each phase has been calculated. With the flow stress for each phase  $\sigma_\alpha$  and  $\sigma_\beta$  calculated from Eq. (6), the flow stress of the dual phase material can be easily obtained from the mixture rule as,

$$\sigma_{\alpha+\beta} = \eta\sigma_\alpha + (1 - \eta)\sigma_\beta \quad (13)$$

where  $\eta$  is the volume fraction of the  $\alpha$  phase. In the current study, we assume that only the initial strength  $A$  is different in  $JC$  model for different phases. This is a reasonable assumption because the biggest difference between the  $\alpha$  and  $\beta$  phase is the initial yield strength. The material initial yield stress  $A$  is a strong function of the grain size, which could be described by the Hall-Petch equation, as

$$A = A_{hp} + K_{hp}D^{-0.5} \tag{14}$$

where  $A_{hp}$  and  $K_{hp}$  are the Hall-Petch parameters. For the *Ti-6Al-4V* material, the  $A$  values are obtained by a linear regression method from the experimental flow stress data at different volume fraction of  $\beta$  phase provided in Zhang’s [34] paper, as listed in Table 3 [36].

Also, the modified  $JC$  model parameters of AISI 4130 are listed in Table 4. The modified  $JC$  model is implemented as the user subroutine in the finite element code. A detailed implementation of the grain growth and phase transformation is shown in Fig. 4.

**Table 3** Modified  $JC$  model parameters for  $\alpha$  and  $\beta$  phases of *Ti-6Al-4V*

Phase	$A_{hp}$	$K_{hp}$	B	n	C	m	$T_m$ (°)	$\dot{\epsilon}_0$
$\alpha$	517.31	201.68	683.10	0.47	0.035	1	1668	1
$\beta$	296.55	100.84	314.55	0.47	0.035	1	1668	1

**Table 4** Modified  $JC$  model parameters for AISI 4130 alloy steel

$A_{hp}$	$K_{hp}$	B	C	m	n	$T_m$ (°)	$\dot{\epsilon}_0$
574.58	112	750	0.008	1	0.25	1432	1

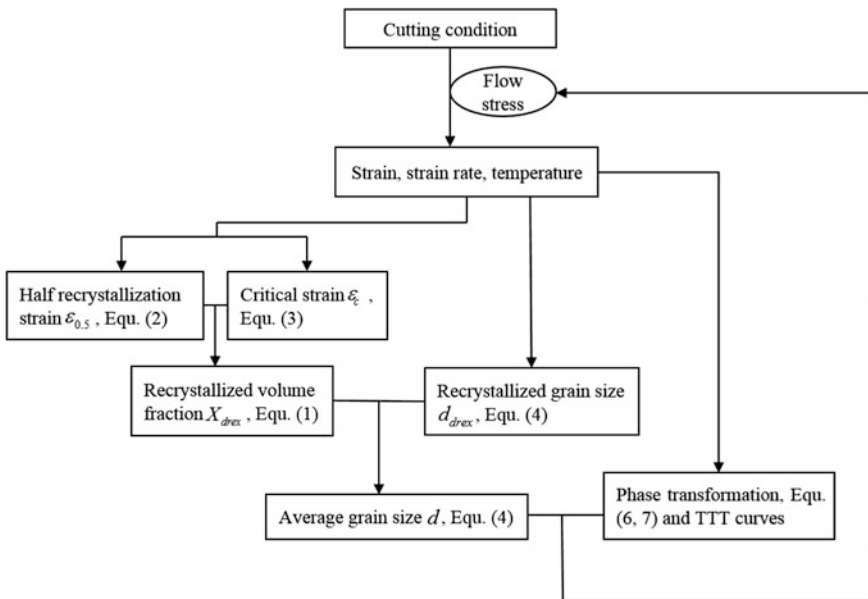


**Fig. 4** Schematic illustration of the grain growth and phase transformation implementation

## 4 Phase Transformation and Grain Size Prediction

The grain size evolution and phase transformation in the orthogonal turning process are predicted with the above proposed method. The initial material average grain size is  $15\ \mu\text{m}$ , the  $\alpha$  phase volume fraction is 95%. The cutting insert with a tool edge radius of  $5\ \mu\text{m}$  is used. The rake angle in orthogonal turning is  $5^\circ$ . A cutting speed at 55 m/min is used, as reported in a previous research. The predicted average grain size and  $\alpha$  phase volume fraction are plotted in Fig. 4. The machined surface has slight grain refinement, shown in Fig. 5a. Also, significant amount of  $\beta$  phase generated in both the chip and machined workpiece surface, as indicated in Fig. 5b.

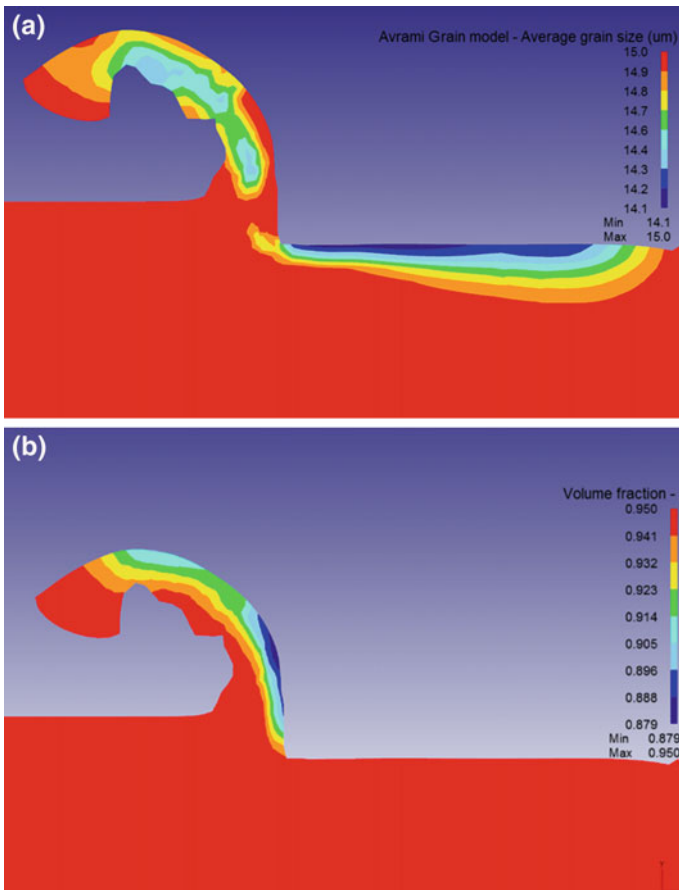


**Fig. 5** The predicted grain size (a) and volume fraction of  $\alpha$  phase (b) at cutting speed of 55 m/min, depth of cut 0.076 mm

### 5 The Force Prediction

For the machining of *Ti-6Al-4V*, four sets of different orthogonal turning conditions are used here to validate the proposed model. The cutting insert edge radius is measured to be 13  $\mu\text{m}$ . A cutting speed is selected as 0.5 m/s. Tool rake angle is  $8^\circ$ . The width of cut is fixed at 3.8 mm. The predicted force and measurement data are plotted in Fig. 6 for comparison at two different depth of cut. The model with a grain size evolution resolves a better prediction compared with the traditional *JC* flow stress model. By varying the rake angle from  $8^\circ$  to  $15^\circ$ , with a constant cutting speed, the predicted forces are plotted in Fig. 7. A better prediction is also observed in Fig. 7.

Similarly, the application of the microstructure sensitive flow stress model is implemented in the hard turning of AISI 4130 steel for further validation. Five machining experiments of AISI 4130 are used for the force model validation. A thin wall cylindrical workpiece is used. The wall thickness is measured to be 4.775 mm.

**Fig. 6** Cutting force  $F_c$  (a) and ploughing force  $F_t$  (b) with a rake angle of  $8^\circ$  at different depth of cut

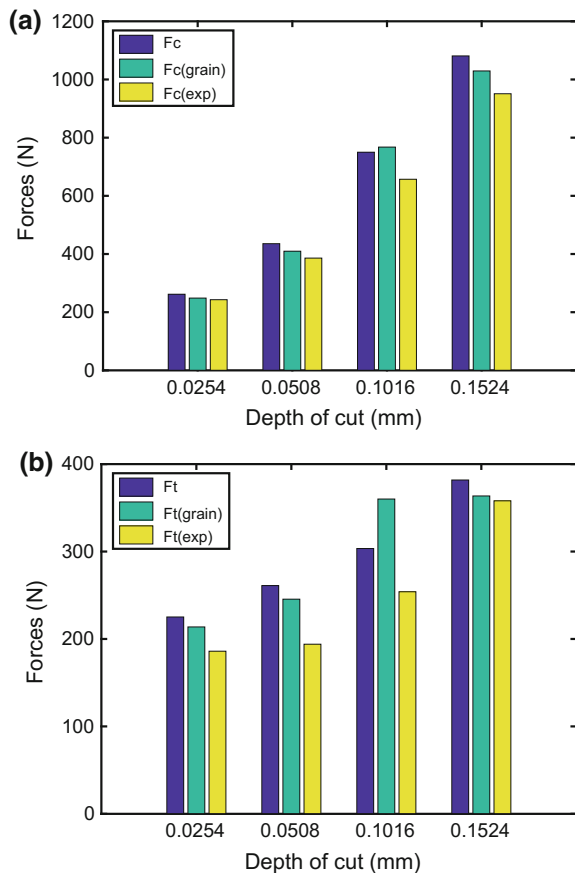
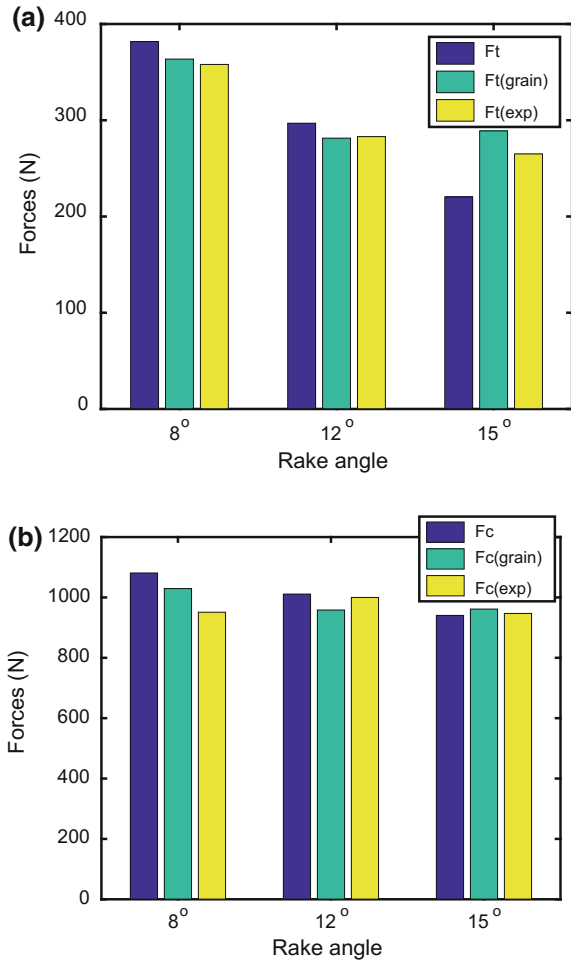


**Fig. 7** Cutting force  $F_c$  (a) and ploughing force  $F_t$  (b) at a depth of cut 0.153 mm with different rake angles



A Sandvik tungsten carbide tool is mounted to a tool holder to achieve a 5° rake angle and 11° relief angle.

The cutting speed is fixed at 1.049 m/s, the machining forces are plotted as a function of different feed rates, as shown in Fig. 8. To show the microstructure effects on the machining force prediction. The predicted force without a grain size consideration is also imposed in Fig. 8.

The grain model obtains a closer approximation to the measurement data, as compared with the traditional model. A general trend is found that, both the cutting force  $F_c$  and  $F_t$  will increase monotonically with the increasing feed rate. Additionally, to investigate the effect of cutting speed on the machining forces, the turning feed rate is fixed at 0.0508 mm/rev by varying the cutting speed. The  $F_c$  and  $F_t$  are plotted as a function of cutting speed, as shown in Fig. 9.

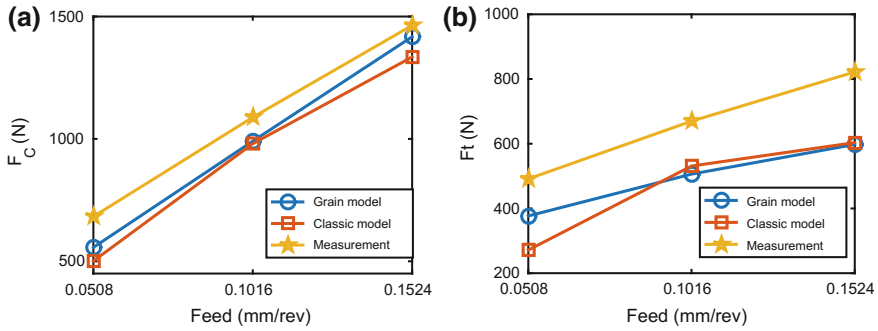


**Fig. 8** When cutting speed is fixed at 1.049 m/s, the cutting forces  $F_C$  (a) and  $F_t$  (b) as a function of feed rate

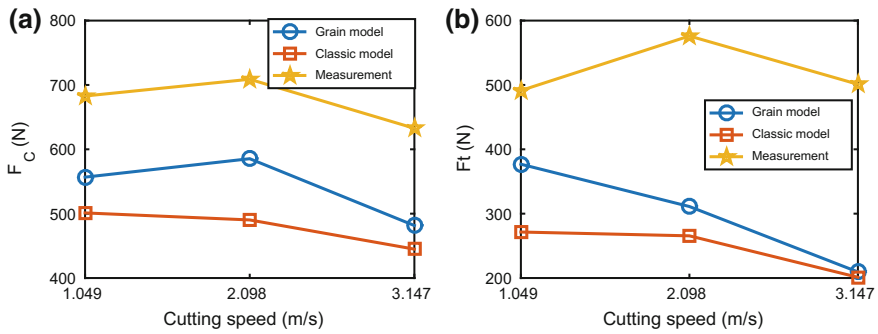


**Fig. 9** When feed rate is fixed at 0.0508 mm/rev, the cutting forces  $F_C$  (a) and  $F_t$  (b) as a function of cutting speed

Both the  $F_t$  and  $F_C$  follows the similar trend, as when the cutting speed increase, the force first increases and then decreases. Also, the grain model gives a better prediction compared with the classic model.

## 6 Residual Stress Prediction

By implementing the proposed microstructure sensitive flow stress model, the residual stress on the machined workpiece surface could be predicted with an analytical model. The residual stress prediction is first applied for the *Ti-6Al-4V* material. With a constant feed rate of 0.1 mm/rev, depth of cut 0.1 mm and cutting speed at 26.4 m/min, the residual stress is plotted as a function of distance from the machined surface into the workpiece, as shown in Fig. 10. Since a two-dimensional stress distribution assumption is used, in which the stress in the workpiece axial direction is negligible. The largest magnitude of stress value is found to be on the

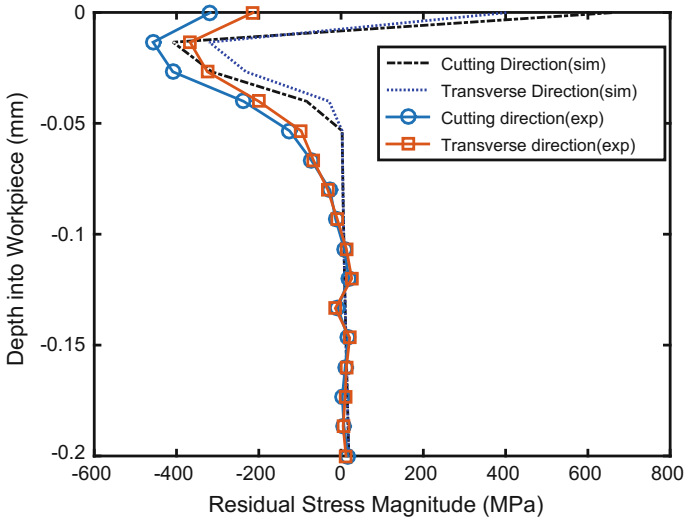
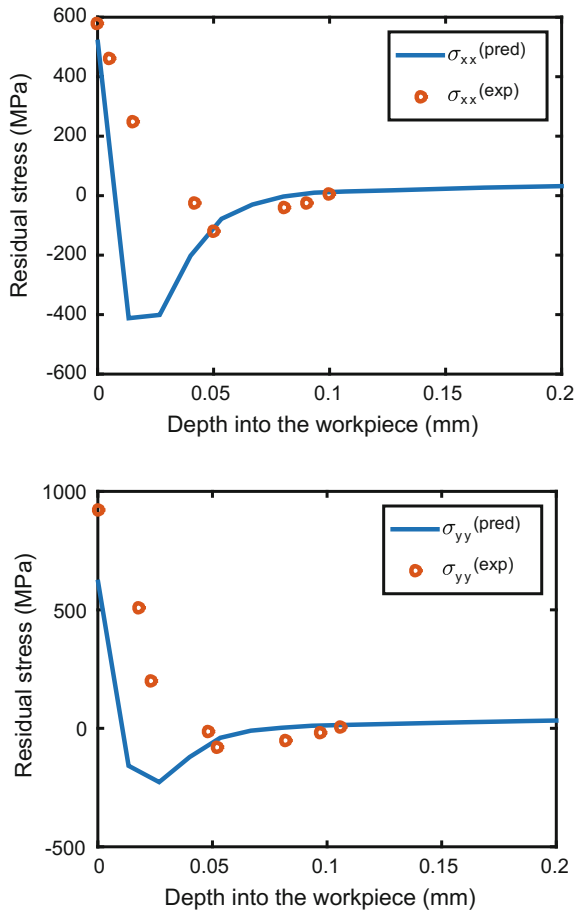


**Fig. 10** Prediction and measured residual stress at feed rate  $100 \mu\text{m}/\text{rev}$ , cutting speed  $26.4 \text{ m}/\text{min}$ , depth of cut of  $100 \mu\text{m}$

machined surface. With the increasing depth into the workpiece, the tensile residual stress first decrease and change to compressive at a certain depth. After that, the compressive residual stress reaches its peak value and then decreases to zero. When the depth is around  $0.1 \text{ mm}$ , the magnitude of the residual stress is around zero. So in the current machining condition, the residual stress affected depth is around  $100 \mu\text{m}$ . A good agreement is found between the prediction and experimental measurement from Ratchev et al. [37]. However, large discrepancy is found on the surface, where the prediction shows tensile residual stress, but the experimental measurements show the compressive stress. Those errors could be from the oxidation on the machined surface.

For the residual stress in the cutting direction  $\sigma_{xx}$ , with the increasing depth into workpiece, the tensile residual stress changes to compressive. After the peak value of compressive residual stress occurs, the compressive residual stress gradually reduces to zero. A good agreement between the measurement data and prediction is found in both  $\sigma_{xx}$  and  $\sigma_{yy}$  (Fig. 11).

**Fig. 11** Comparison of predicted residual stress between experimental measurement at cutting speed of 1.049 m/s, depth of cut = 0.0508 mm, width of cut = 4.775 mm



## 7 Conclusion

A materials-affected manufacturing computational framework for the material dynamic recrystallization and phase transformation in the machining process is proposed in the current work. The *JMAK* model is used for the explicit grain size evolution calculation by assuming an isothermal condition. With the temperature history input, phase composition of different phases is calculated from the TTT curve and Avrami equations. A modified *JC* flow stress model is developed by considering the grain size and phase volume fraction effects. The proposed model is applied in the case study of *Ti-6Al-4V* and AISI 4130 steel alloys for the machining forces and residual stresses predictions. Experimental data are provided for the model validation. Better force and residual stress predictions are obtained compared with the traditional model. The proposed framework could provide a machining process optimization scheme at a microstructural level.

## References

1. Lim EM, Menq CH (1997) Integrated planning for precision machining of complex surfaces. Part 1: cutting-path and feedrate optimization. *Int J Mach Tools Manuf* 37(1):61–75
2. Cheung CF, Lee WB (2000) A multi-spectrum analysis of surface roughness formation in ultra-precision machining. *Precision Engineering* 24(1):77–87
3. Picard YN et al (2003) Focused ion beam-shaped microtools for ultra-precision machining of cylindrical components. *Precis Eng* 27(1):59–69
4. Ulutan D, Ozel T (2011) Machining induced surface integrity in titanium and nickel alloys: a review. *Int J Mach Tools Manuf* 51(3):250–280
5. Pan Z et al (2016) Analytical model for force prediction in laser-assisted milling of IN718. *Int J Adv Manuf Technol*. doi:[10.1007/s00170-016-9629-6](https://doi.org/10.1007/s00170-016-9629-6)
6. Lei S, Liu W (2002) High-speed machining of titanium alloys using the driven rotary tool. *Int J Mach Tools Manuf* 42(6):653–661
7. Pan Z et al (2017) Modeling of Ti–6Al–4V machining force considering material microstructure evolution. *Int J Adv Manuf Technol*. doi:[10.1007/s00170-016-9964-7](https://doi.org/10.1007/s00170-016-9964-7)
8. Fergani O et al (2016) Microstructure texture prediction in machining processes. *Procedia CIRP* 46:595–598
9. Ghosh S, Kain V (2010) Microstructural changes in AISI 304L stainless steel due to surface machining: effect on its susceptibility to chloride stress corrosion cracking. *J Nucl Mater* 403(1):62–67
10. Barbacki A, Kawalec M, Hamrol A (2003) Turning and grinding as a source of micro structural changes in the surface layer of hardened steel. *J Mater Process Technol* 133(1):21–25
11. Lu C (2008) Study on prediction of surface quality in machining process. *J Mater Process Technol* 205(1):439–450
12. Zhipeng Pan AT, Shih DS, Garmestani H, Liang SY (2017) The Effects of Dynamic Evolution of Microstructure on Machining Forces. In: Proceedings of the institution of mechanical engineers, Part B: Journal of Engineering Manufacture
13. Xu HH, Jahanmir S (1994) Effect of microstructure on abrasive machining of advanced ceramics. In: A collection of papers presented at the 96th annual meeting and the 1994 fall meetings of the materials and equipment/Whitewares/Refractory Ceramics/Basic Science: Ceramic Engineering and Science Proceedings, Vol. 16, Issue 1. 1995. Wiley Online Library
14. Chou YK, Evans CJ (1999) White layers and thermal modeling of hard turned surfaces. *Int J Mach Tools Manuf* 39(12):1863–1881
15. Swaminathan S et al (2007) Severe plastic deformation of copper by machining: microstructure refinement and nanostructure evolution with strain. *Scripta Mater* 56(12):1047–1050
16. Filip R et al (2003) The effect of microstructure on the mechanical properties of two-phase titanium alloys. *J Mater Process Technol* 133(1):84–89
17. Gil F et al (2001) Formation of  $\alpha$ -Widmanstätten structure: effects of grain size and cooling rate on the Widmanstätten morphologies and on the mechanical properties in Ti–6Al–4V alloy. *J Alloy Compd* 329(1):142–152
18. Kugler G, Turk R (2004) Modeling the dynamic recrystallization under multi-stage hot deformation. *Acta Mater* 52(15):4659–4668
19. Suárez A et al (2004) Modeling of phase transformations of Ti–6Al–4V during laser metal deposition. *Physics Procedia* 12:666–673
20. Malinov S et al (2001) Differential scanning calorimetry study and computer modeling of  $\beta \Rightarrow \alpha$  phase transformation in a Ti–6Al–4V alloy. *Metall Mat Trans A* 32(4):879–887
21. Ducato A, Fratini L, Micari F (2013) Prediction of phase transformation of Ti–6Al–4V titanium alloy during hot-forging processes using a numerical model. In: Proceedings of the institution of mechanical engineers, Part L: Journal of Materials Design and Applications, p. 1464420713477344

22. Jiles D (1988) The effect of compressive plastic deformation on the magnetic properties of AISI 4130 steels with various microstructures. *J Phys D Appl Phys* 21(7):1196
23. Ji X et al (2014) Modeling the effects of minimum quantity lubrication on machining force, temperature, and residual stress. *Mach Sci Technol* 18(4):547–564
24. Grum J, Kisin M (2003) Influence of microstructure on surface integrity in turning—Part II: the influence of a microstructure of the workpiece material on cutting forces. *Int J Mach Tools Manuf* 43:1545–1551
25. Gibbs RK, Hodgson PD (1992) A mathematical model to predict the mechanical properties of the hot rolled C–Mn and microalloyed steels. *ISIJ Int* 32(12):10
26. Hawbolt EB, Sun WP (1997) Comparison between Static and Metadynamic Recrystallization an application to the hot rolling of steels. *ISIJ Int* 37(10):1000–1009
27. Sajadi SV, Ketabchi M, Nourani MR (2010) Hot deformation characteristics of 34CrMo4 steel. *J Iron Steel Res Int* 17(12):65–69
28. Xia Ji XZ, Li Beizhi, Liang Steven Y (2014) Modeling the effects of minimum quantity lubrication on machining force, temperature, and residual stress. *Mach Sci Technol Int J* 18(4):547–564
29. Srinivasa YV, Shunmugam MS (2013) Mechanistic model for prediction of cutting forces in micro end-milling and experimental comparison. *Int J Mach Tools Manuf* 67:18–27
30. Kim DH, Lee CM (2014) A study of cutting force and preheating-temperature prediction for laser-assisted milling of Inconel 718 and AISI 1045 steel. *Int J Heat Mass Transf* 71:264–274
31. Roucoules C, Hodgson P (1995) Post-dynamic recrystallisation after multiple peak dynamic recrystallisation in C–Mn steels. *Mater Sci Technol* 11(6):548–556
32. Johnson GR, Cook WH (1983) A constitutive model and data for metals subjected to large strains, high strain rates and high temperatures. In: *Proceedings of the 7th international symposium on ballistics*, The Hague, The Netherlands
33. Calamaz M, Coupard D, Girof F (2008) A new material model for 2D numerical simulation of serrated chip formation when machining titanium alloy Ti–6Al–4V. *Int J Mach Tools Manuf* 48(3):275–288
34. Zhang X, Shivpuri R, Srivastava A (2014) Role of phase transformation in chip segmentation during high speed machining of dual phase titanium alloys. *J Mater Process Technol* 214(12):3048–3066
35. Shivpuri R et al (2002) Microstructure-mechanics interactions in modeling chip segmentation during titanium machining. *CIRP Ann Manuf Technol* 51(1):71–74
36. Pan Z et al (2016) Prediction of machining-induced phase transformation and grain growth of Ti–6Al–4V alloy. *Int J Adv Manuf Technol* 87(1):859–866
37. Ratchev S et al (2011) Mathematical modelling and integration of micro-scale residual stresses into axisymmetric FE models of Ti–6Al–4V alloy in turning. *CIRP J Manuf Sci Technol* 4(1):80–89